# Theoretical study of detection of a dipole emitter through an objective with high numerical aperture

**Jörg Enderlein**

*Institute of Analytical Chemistry, Chemo- and Biosensors, Regensburg University, PF 10 10 42, D-93040 Regensburg, Germany*

Received November 30, 1999

The problem of detecting electric dipole emitters (such as a fluorescing molecule) through a microscope objective with a high numerical aperture is considered. Exact vector-wave-optics results of the field distribution of the electromagnetic field in image space are derived. On the basis of these results, the collection-efficiency function (CEF) is calculated. This calculation is compared with a semigeometric approximation of the CEF, for which a new analytical formula is presented. The derived results are important for applications such as fluorescence correlation spectroscopy and single-molecule fluorescence detection with a confocal microscope.

*OCIS codes:* 300.2530, 300.6280, 260.1960, 260.2110, 180.1790.

In recent years fluorescence detection and spectroscopy of single molecules in liquid solution under ambient conditions have seen tremendous development (see, e.g., Refs. 1–4). One of the most widely used techniques for detecting single molecules in solution is so-called confocal laser epifluorescence microscopy.[5,6] In this technique a laser beam is focused through a microscope objective with a high numerical aperture into a diffraction-limited spot within the solution where fluorescing molecules are present at sufficiently low concentration. This laser beam excites the fluorescence of individual molecules diffusing through its focus. The resulting burst of fluorescence photons is collected by the same objective (epifluorescence setup) and detected, after passing appropriate emission filters and a circular confocal aperture, by a sensitive photoelectron detector (e.g., a single-photon avalanche diode). The introduction of a confocal aperture into the detection path results in tight restriction of the detection volume in the direction of the optical axis. The extent of this volume perpendicular to the optical axis is determined by the beam-waist diameter of the focused laser beam. The restriction of the detection volume is crucial for reducing the background signals that are due mainly to Rayleigh and Raman scattering of the laser beam by the solvent.

In many applications exact knowledge of the form of the detection volume is crucial. For example, in fluorescence correlation spectroscopy[7] one can extract information about molecular properties, such as translational and rotational diffusion and reaction kinetics, by evaluating the fluctuations of the detected fluorescence by a temporal autocorrelation of the recorded photon counts. Extracting quantitative information from these autocorrelations requires exact knowledge of the intensity distribution of the exciting laser light and of the collection-efficiency function (CEF). The CEF describes the efficiency with which the emission of a point dipole is detected by a photoelectron detector behind the confocal aperture, depending on the position of that dipole in object space.

Whereas the spatial distribution of the electromagnetic field near the laser focus in object space was exactly calculated by Wolf[8] and Richards and Wolf[9] in their seminal work, an exact vector-wave treatment of the CEF of a dipole emitter is still lacking. In Ref. 10, Qian and Elson proposed a semigeometric-optics approximation of this function.

In our calculations it is assumed that the objective has perfect imaging properties. The geometry of the studied situation is shown schematically in Fig. 1. In the object space of the objective a dipole emitter is placed at the focal point of the objective. In image space a confocal aperture is positioned exactly at the image plane. Following Wolf and Richards, the electric field amplitude in image space near the focal plane is given by

$$\mathbf{E} = \int_0^{\eta'_{\max}} \mathrm{d}\eta' \sin\eta' \int_0^{2\pi} \mathrm{d}\psi \sqrt{\frac{\cos\eta'}{\cos\eta}} [\hat{e}'_{\perp}(\mathbf{p}\hat{e}_{\perp}) + \hat{e}_{\parallel}(\mathbf{p}\hat{e}_{\parallel})][\exp(ikR)/R]\exp(ik'\hat{s}'\mathbf{r}'), \quad (1)$$

where $\mathbf{p}$ is the dipole vector, $k$ and $k'$ are the wave numbers of the light in object and image space, respectively, $R$ is the distance from the dipole emitter to a point (determined by $\eta$ and $\psi$) on a reference sphere around the object-space focus (see Fig. 1), $\mathbf{r}'$ is the position of the target point in image space, where the electric field amplitude is calculated, the angles $\eta$ and $\eta'$ are shown in Fig. 1, and the following unit vectors are defined:

$$\begin{aligned} \hat{e}_{\perp} &= (\cos\psi\cos\eta, \sin\psi\cos\eta, -\sin\eta), \\ \hat{e}_{\parallel} &= (-\sin\psi, \cos\psi, 0), \\ \hat{e}'_{\perp} &= (\cos\psi\cos\eta', \sin\psi\cos\eta', \sin\eta'), \\ \hat{s}' &= (-\sin\eta'\cos\psi, -\sin\eta'\sin\psi, \cos\eta'), \end{aligned} \quad (2)$$

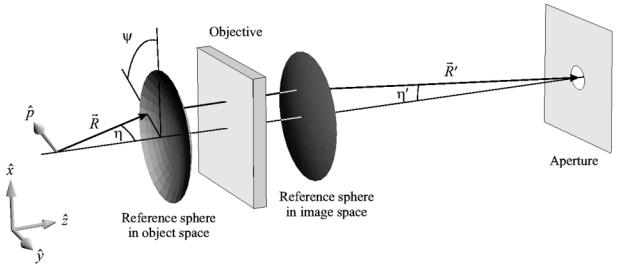


Fig. 1. Schematic of the imaging geometry of the dipole.

0146-9592/00/090634-03$15.00/0 

with the angle $\psi$ as shown in Fig. 1. The connection between angles $\eta$ and $\eta'$ is given by the magnification $M$ of the objective through $\tan\,\eta = M\,\tan\,\eta'$, and the integration limit of $\eta'$ is defined through the value of the numerical aperture (NA) and the refractive index $n$ of the object space through

$$\eta'_{\max} = \arctan\left(\frac{\mathrm{NA}}{M\sqrt{n^2 - \mathrm{NA}^2}}\right). \tag{3}$$

A relation similar to that for the electric field amplitude holds for the amplitude of the magnetic field,

$$\mathbf{B} = n' \int_0^{\eta'_{\max}} \mathrm{d}\eta'\,\sin\,\eta' \int_0^{2\pi} \mathrm{d}\psi \sqrt{\frac{\cos\,\eta'}{\cos\,\eta}}\,[\hat{e}_{|}(\mathbf{p}\hat{e}_{\perp}) - \hat{e}'_{\perp}(\mathbf{p}\hat{e}_{|})][\exp(ikR)/R]\exp(ik'\hat{s}'\mathbf{r}'), \tag{4}$$

where $n'$ is the refractive index of the image space. For the scalar product $\hat{s}'\mathbf{r}'$, the following relation holds:

$$\begin{aligned}\hat{s}'\mathbf{r}' &= \hat{s}'(\mathbf{R}' + \boldsymbol{\rho}' + \mathbf{z}') \\ &= R' - \rho'\,\sin\,\eta'\,\cos(\psi - \phi') + z'\,\cos\,\eta',\end{aligned} \tag{5}$$

where $\mathbf{R}'$ is a vector connecting the point with angles $\eta'$ and $\psi$ on the reference sphere around the image-space focus with that focus (see Fig. 1), $\boldsymbol{\rho}'$ is a vector pointing from the optical axis to the target point (perpendicular to the optical axis), $z'$ is the distance of the target point from the focus along the optical axis, and $\phi'$ is the angle between $\boldsymbol{\rho}'$ and the unit vector $\hat{x}$. The integration over the variable $\psi$ in Eqs. (1) and (4) can be done analytically, and after some algebraic transformations one obtains

$$E_a = 2\pi\,\frac{\exp(ikR + ik'R')}{R} \int_0^{\eta'_{\max}} \mathrm{d}\eta'\,\sin\,\eta' \sqrt{\frac{\cos\,\eta'}{\cos\,\eta}} \times G^E_{ab}(\eta, \phi', \rho')p_b \exp(ik'z'\,\cos\,\eta'), \tag{6}$$

where the subscripts $a$ and $b$ denote Cartesian components $x$, $y$, and $z$, summation over repeating indices is assumed, and the components of the tensor $G^E_{ab}$ are given by

$$\begin{aligned}
G^E_{xx} &= \frac{1}{2}(1 + \cos\,\eta'\,\cos\,\eta)J_0 + \frac{1}{2}(1 - \cos\,\eta'\,\cos\,\eta)J_2\,\cos\,2\phi', \\
G^E_{xy} &= G^E_{yx} = \frac{1}{2}(1 - \cos\,\eta'\,\cos\,\eta)J_2\,\sin\,2\phi', \\
G^E_{xz} &= -i\,\cos\,\eta'\,\sin\,\eta J_1\,\cos\,\phi', \\
G^E_{yy} &= \frac{1}{2}(1 + \cos\,\eta'\,\cos\,\eta)J_0 - \frac{1}{2}(1 - \cos\,\eta'\,\cos\,\eta)J_2\,\cos\,2\phi', \\
G^E_{yz} &= -i\,\cos\,\eta'\,\sin\,\eta J_1\,\sin\,\phi', \\
G^E_{zx} &= i\,\sin\,\eta'\,\cos\,\eta J_1\,\cos\,\phi', \\
G^E_{zy} &= i\,\sin\,\eta'\,\cos\,\eta J_1\,\sin\,\phi', \\
G^E_{zz} &= -\sin\,\eta'\,\sin\,\eta J_0,
\end{aligned} \tag{7}$$

where $J_{0,1,2}$ denote Bessel functions of the first kind[11] with the argument $k'\rho'\,\sin\,\eta'$. A result similar to that of Eq. (6) holds for the components $B_a$ of the magnetic field amplitude, but the result is multiplied by $n'$ and by a different tensor $G^B_{ab}$:

$$\begin{aligned}
G^B_{xx} &= -G^B_{yy} = \frac{1}{2}(\cos\,\eta - \cos\,\eta')J_2\,\sin\,2\phi', \\
G^B_{xy} &= -\frac{1}{2}(\cos\,\eta + \cos\,\eta')J_0 - \frac{1}{2}(\cos\,\eta - \cos\,\eta')J_2\,\cos\,2\phi', \\
G^B_{xz} &= iJ_1\,\sin\,\eta\,\sin\,\phi', \\
G^B_{yx} &= \frac{1}{2}(\cos\,\eta + \cos\,\eta')J_0 - \frac{1}{2}(\cos\,\eta - \cos\,\eta')J_2\,\cos\,2\phi', \\
G^B_{yz} &= -iJ_1\,\sin\,\eta\,\cos\,\phi', \\
G^B_{zx} &= -iJ_1\,\sin\,\eta'\,\sin\,\phi', \\
G^B_{zy} &= iJ_1\,\sin\,\eta'\,\cos\,\phi', \\
G^B_{zz} &= 0.
\end{aligned} \tag{8}$$

Until now, only dipole positions exactly at the focus of the objective have been considered. However, for the direct vicinity of that focus the following simple rule applies: The field amplitudes in image space for a dipole shifted by a vector $\boldsymbol{\rho}$ away from the optical axis and a distance $z$ along the optical axis are given by the field distribution for the in-focus dipole but at positions in image space that are shifted by the vector $\boldsymbol{\rho}' = -M\boldsymbol{\rho}$ away from the optical axis and the distance $z' = M^2 z$ along the optical axis. Thus, Eqs. (6)–(8) contain full information about the field amplitudes in image space for an arbitrary dipole position in object space.

Finally, to obtain the energy flow through the confocal aperture one has to calculate the Poynting vector, which is proportional to $\mathbf{E} \times \mathbf{B}^*$ (the asterisk denotes complex conjugation). The integral of the vector's $z$ component over the aperture area yields the energy flux through the aperture, which is a direct measure of the detection efficiency for the given dipole position and orientation.

As an example that is of practical relevance, the CEF of an objective with 1.2 NA and magnification $M = 100$ is numerically studied. The refractive indices of the object and image space are assumed to be 1.33 (water) and 1.0 (air), respectively. The back image of the confocal aperture in object space is assumed to have a radius $a$ of half of the vacuum wavelength $\lambda$ of the emitted light, $a = \lambda/2$. The computational result is shown in Fig. 2(a), in which the CEF is averaged over all possible dipole orientations. For comparison, the semigeometric-optics approximation of Qian and Elson is shown in Fig. 2(b). Their CEF is computed according to

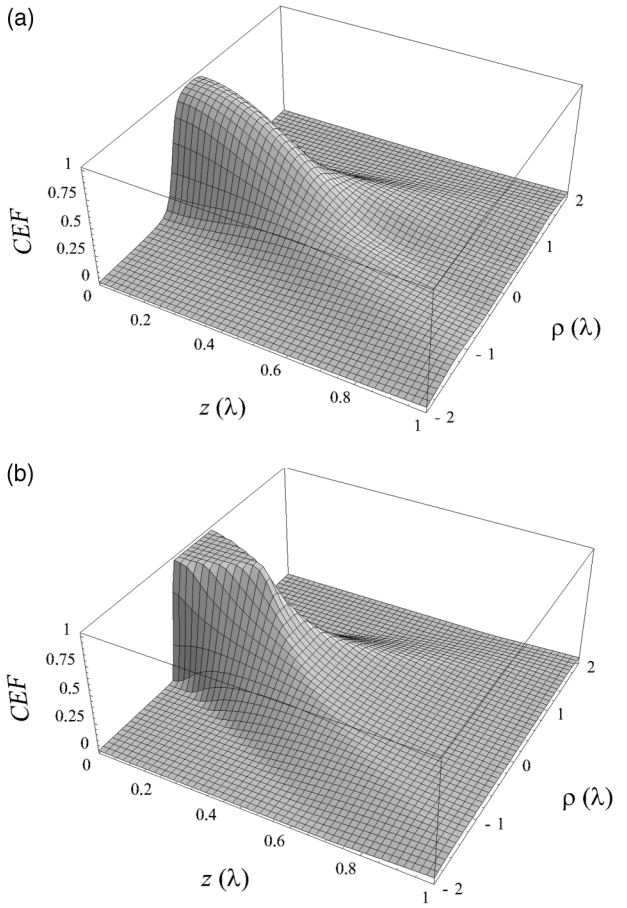


Fig. 2. CEF as computed by (a) the full wave-vector approach and (b) the semigeometric approximation of Qian and Elson.

$$\mathrm{CEF}(\rho, z) = \int \frac{\mathrm{circ}(\rho_a/a)\mathrm{circ}[|\boldsymbol{\rho}_a - \boldsymbol{\rho}|/u(z)]}{\pi u^2(z)}\,\mathrm{d}\boldsymbol{\rho}_a\,, \tag{9}$$

where circ denotes an aperture function of 1 for argument values smaller than 1 and of 0 otherwise. Here $u(z) = w_0[1 + (\lambda z/\pi n w_0^2)^2]^{1/2}$ and $w_0 = \lambda/\pi n \tan \eta_{\max}$, with $\eta_{\max}$ being the maximum angle of collection of the objective in object space, $\eta_{\max} = \arcsin \mathrm{NA}/n$. The integration variable $\boldsymbol{\rho}_a$ in Eq. (9) is perpendicular to the optical axis, and the integration extends over the whole two-dimensional $\boldsymbol{\rho}_a$ plane. The integration can be done analytically, leading to

$$\mathrm{CEF}(\rho, z) = 0, \quad \rho \geq u + a$$

$$\mathrm{CEF}(\rho, z) = \max(a, w_0)^2(\theta_1 a^2 + \theta_2 u^2 - \Delta)/(\pi a^2 u^2), \quad |u - a| < \rho < u + a$$

$$\mathrm{CEF}(\rho, z) = \max(a, w_0)^2/\max(a, u)^2, \quad \rho \leq |u - a|\,, \tag{10}$$

where, for brevity, the argument of the function $u$ has been omitted, and the abbreviations

$$\theta_1 = \arccos[(a^2 + \rho^2 - u^2)/2a\rho]\,,$$

$$\theta_2 = \arccos[(u^2 + \rho^2 - a^2)/2u\rho]\,, \tag{11}$$

$$\Delta = \frac{[(a + \rho + u)(-a + \rho + u)(a - \rho + u)(a + \rho - u)]^{1/2}}{2}$$

have been introduced.

As can be seen from Fig. 2, the semigeometric-optics approximation and the exact wave-optics result are remarkably similar. Of course, the wave-optics result avoids the sharp edges and the flat plateau that are seen in the geometric-optics case. However, if one computes an effective volume of collection as

$$V = \int_0^\infty \mathrm{d}\rho\,\rho \int_{-\infty}^{\infty} \mathrm{d}z\mathrm{CEF}(\rho, z)\,, \tag{12}$$

the results for the wave- and the geometric-optics calculations coincide by better than 5%.

I thank Martin Böhmer and Thomas Ruckstuhl for many inspiring discussions. I would especially like to thank Eike Stedefeldt for his enduring and exceedingly helpful support of my work. My e-mail address is joerg.enderlein@chemie.uni-regensburg.de.

## References

1. M. D. Barnes, W. B. Whitten, and J. M. Ramsey, Anal. Chem. **67,** 418A (1995).
2. R. A. Keller, W. P. Ambrose, P. M. Goodwin, J. H. Jett, J. C. Martin, and M. Wu, Appl. Spectrosc. **50,** 12A (1996).
3. S. M. Nie and R. N. Zare, Annu. Rev. Biophys. Biomol. Struct. **26,** 567 (1997).
4. J. Enderlein, W. P. Ambrose, P. M. Goodwin, and R. A. Keller, in *Microsystem Technology: A Powerful Tool for Biomolecular Studies*, M. Köhler, T. Mejevaia, and H. P. Saluz, eds. (Birkhäuser, Basel, Switzerland, 1999), p. 311.
5. S. Inoue, in *Handbook of Biological Confocal Microscopy*, 2nd ed., J. B. Pawley, ed. (Plenum, New York, 1995), p. 1.
6. R. H. Webb, Rep. Prog. Phys. **59,** 427 (1996).
7. N. L. Thompson, in *Topics in Fluorescence Spectroscopy*, J. R. Lakowicz, ed. (Plenum, New York, 1991), Vol. 1, p. 337.
8. E. Wolf, Proc. R. Soc. London Ser. A **253,** 349 (1959).
9. B. Richards and E. Wolf, Proc. R. Soc. London A **253,** 358 (1959).
10. H. Qian and E. L. Elson, Appl. Opt. **30,** 1185 (1991).
11. M. Abramowitz and I. A. Stegun, eds., *Handbook of Mathematical Functions* (Deutsch, Thun, Switzerland, 1984).